ELSEVIER

Contents lists available at ScienceDirect

Ceramics International

journal homepage: www.elsevier.com/locate/ceramint





Microstructure evolution and wear resistance of in-situ synthesized (Ti, Nb) C ceramic reinforced Ni204 composite coatings

Yu Zhao ^{a,b}, Liaoyuan Chen ^c, Jiayu Sun ^d, Wenzheng Wu ^{a,b,*}, Tianbiao Yu ^c

- ^a School of Mechanical and Aerospace Engineering, Jilin University, Changchun, 130025, China
- ^b Chongqing Research Institute, Jilin University, Chongqing, 401133, China
- ^c School of Mechanical Engineering and Automation, Northeastern University, Shenyang, 110819, China
- ^d Deformation Processing Institute for Materials Research, Tohoku University, Sendai, 980-8577, Japan

ARTICLE INFO

Keywords: Ti/C/NbC Ni204 alloy Laser cladding Microhardness Friction coefficient

ABSTRACT

Poor mechanical properties of Ni alloy hinder its widespread application in the industrial. In order to enhance its performance, Ni204-based composite coatings reinforced with in-situ TiC and (Ti, Nb)C particles were investigated and successfully built on 45 steel alloy via laser cladding technology. The strengthening phase characteristics, microstructure evolution, and mechanical properties of the samples were examined and analyzed. By doping Ti and C particles into the NbC–Ni composite coatings, the large lump structure of NbC was effectively eliminated. The alternative formation of TiC and NbC promoted the in-situ generation of the multiphase (Ti, Nb) C and further prevented the NbC from agglomerating. Therefore, the problem of TiC particles floating has been effectively alleviated. The microhardness is up to 1.53 higher than that of the original Ni204 coating. Compared with the mass fraction ratio of Ti/C/NbC is 7:2:21 composite coating, the wear resistance of the composite coating (the addition of NbC is 30%) is improved by around 11 times. The composite coating has excellent combination property when the mass fraction ratio of Ti/C/NbC is 4:1:5. This work provides insight into the Ni204-based composite coatings by ceramic reinforcement.

1. Introduction

As a novelty technology, laser cladding is applied widely in the surface strengthening and surface repair of manufacturing, healthcare, electronics, and other fields. The laser cladding components have excellent density and low dilution rate, but the lower hardness and severe wear, and short service life for some metal materials themselves limited its application. Therefore, it is crucial to improve the property of the coating. Transition metal carbides (MC), borides, and nitrides have remarkable properties with a high melting point, hardness, thermal conductivity, and electrical conductivity. They have attracted much attention due to their unique properties of the solid solution of ceramics of different metal compounds [1]. Metal matrix composite (MCC) is widespread in surface strengthening by outstanding features, viz., refiner grains, higher hardness, smaller heat-affected zone (HAZ), and excellent wear resistance [2]. Ceramic particles and cemented carbides as one kind of reinforcing phase were used up to now to enhance the properties of coatings. Specifically, the need-like phases can improve the hardness, strength, and chemical stability of composite coating by inhibiting the growth of the grains or replacing the strengthening particles [3–7].

NbC and TiC particles are the common inhibitors and cemented carbides due to their excellent mechanical properties and similar lattice constants [8]. Niobium (Nb) is a highly activated material with a high melting point, low density, and easy bonding to carbon (C) at high temperatures. As the strong carbides formation elements, titanium (Ti) and Nb can in-situ synthesize TiC, NbC and (Ti, Nb) C with C [2]. Ti and C are more approachable to form TiC, the preferentially precipitated TiC can provide nucleation for the formation of more complex carbides [9]. To improve wear resistance, TiC, TiN, B₄C, TiCN, Al₂O₃, TiB₂, and their mixed composite coatings were used in previous research [10–17]. However, the giant difference in thermal expansion coefficient at the interface between the ceramic coating and metal substrate initiates cracks inevitably in the coating during the laser cladding process. Cracks as drawback are usually easy to spread into the substrate, causing coating failure. TiC as reinforcement was added to improve the

^{*} Corresponding author. School of Mechanical and Aerospace Engineering, Jilin University, Changchun, 130025, China E-mail addresses: zhaoyuneu@gmail.com (Y. Zhao), liaoyuanchen1024.neu@gmail.com (L. Chen), sunjiayudewo@gmail.com (J. Sun), wzwu@jlu.edu.cn (W. Wu), tianbiaoyudyx@gmail.com (T. Yu).

performance of composite coating due to its high melting point, excellent hardness, wettability, and fire resistance [12–14,17]. The lower density of TiC than Ni was regarded as the trigger for its floating behavior on the surface of the molten pool during the laser cladding and solidification process, causing uneven-distributed hard phases inside the coating [14,18,19]. TiC and NbC can be complete miscibility to form multi-carbides (Ti, Nb) C, [20]. The more significant density of NbC solved the problem of TiC floating up [19].

Many researchers studied the properties of TiC and NbC composite ceramic coatings to explore the reinforcement mechanism. Zhang et al. [21] fabricated in-situ (Ti, Nb)C composite coating with various Ti: Nb atomic ratios via plasma cladding. When the content of Ti/Nb (at%) equals 7:3, the wear resistance increased about 2.1 fold. Kan et al. [22] investigated the effect of reinforcement with (Nb $_{0.75}$, Ti $_{0.25}$) C on AISI 304 stainless steel composites. Compared to NbC reinforced particles, (Nb_{0.75}, Ti_{0.25}) C significantly refined primary carbide and improved wear resistance. Sun et al. [23] discussed the microstructure and texture characteristics, wear resistance, microhardness, and formation mechanism of Ti-doped NbC particles reinforced Ni-based coating. The results indicate that the properties and microstructure of the coating with Ti: Nb equals 1:1 were most prominent. Piekarski [24] investigated the effect of Ti and Nb on the microstructure and properties of cast austenitic steels, and the simultaneous addition of Ti and Nb decreased yield strength and ultimate strength of the composite coating. Li et al. [2] investigated the formation mechanism and distribution characteristic of (Ti, Nb) C by adding various Ti/Nb molar ratios, and performance reinforcement were most remarkable when Ti/Nb equals 1. The findings were consistent with the results in Sun's study [23]. The enhancement of multiple phases consisting of Ti, Nb, and C is better than single-phase NbC or TiC [22]. The addition of Ti and Nb can significantly limit the carburizing of the alloy. In-situ synthesis can increase the specific strength and modulus of the reinforcing phase [25-28]. Therefore, in-situ synthesized carbide ceramics have cleaner bonding surfaces to the substrate than ex-situ carbide ceramics and the strengthening phases are more uniform and refined [29-31].

In our previous works, the effect of ex-situ TiC, B₄C and TiN particles reinforced Ni204 coatings have been investigated [15,16], the improvement of the mechanical properties was significant. However, the microstructure appears obvious in Chinese-script structures and severe segregation and reunion of ceramic phases. Compared with discrete carbide particles, Chinese-script carbide ceramics can promote crack propagation and are extremely unfavorable to toughness. Then, it is necessary to eliminate these Chinese-script structures [19,32,33]. In this paper, 30% mass fraction of reinforcing particles were added in Ni204 alloy powder, NbC particles were substituted by equal mass Ti and C particles. The microstructure characteristics, strengthening phase distribution and characteristics, and evolution mechanism of in-situ (Ti, Nb) C/Ni204-based coatings built by laser cladding were further investigated. Additionally, the microhardness and wear resistance reinforced by in-situ (Ti, Nb) C were also investigated.

2. Materials and experimental procedures

2.1. Sample preparation

#45 die steel with the size of $100\times100\times10~\text{mm}^3$ was used as the substrate, Ni204 alloy powders with an average diameters of 53–150 μ m, pure NbC powders (99 wt% NbC, average diameters of \geq 150 μ m), pure Ti powders (99.5 wt% Ti, average diameters of 53–150 μ m), pure C

powders (99.95 wt% C, average diameters of 1–4 μ m) were selected as cladding materials. Ni204 alloy powders (Nanjing zhongke yuchen laser technology co., Ltd.) and Ti, C and NbC powders (Aladdin) were used. Table 1 shows the chemical composition of Ni204 powders and #45 die steel. The 30% mass fraction of Ti, C and NbC powders are used in this experiment and list in Table 2, its detailed chemical composition aligns to our previous study [10,15]. Before the experiment, the composite powders were homogeneously mixed using a ball mill machine at 30 rpm for 2 hs [15].

The laser cladding ceramic/Ni204 composite material samples were prepared by a YLP-500 continuous-wave IPG fiber laser. The diameter of the laser beam is 1.1 mm (laser power P is 450 W). The laser head was fixed on the end-effector of the KUKA robot. Argon was chosen as powder feeding gas and shielding gas, and the value of gas flow was set as 8 L min⁻¹ and 15 L min⁻¹, respectively. The experimental parameters used here are given in Table 3. Fig. 1, which was observed by laser confocal microscopy (OLYMPUS LEXTOLS4100), illustrated the cross-section of composite coatings. Coating 2# appeared cracks, and other coatings showed better morphology.

2.2. Phase characterization

The phase constituent of samples were examined by X-ray diffractometer (XRD, X Pertpro) with Cu as the target, 0–20 scanning was adopted from 5° to 90° in 14 min. The microstructure of the coating was characterized by a field emission scanning electron microscope (SEM, Zeiss Ultra Plus, Germany). The detailed sample preparation has been reported in our previous work [15]. The 2D worn surface of composite coatings was observed in their cross-section plane, and it was characterized by laser confocal microscopy (OLYMPUS LEXTOLS4100, Japan). The electron backscatter diffraction (ESBD) equipped on the SEM was employed to investigate the microstructure characteristics. Energy dispersive spectrometer (EDS) equipped on the SEM was carried out to analyze the energy spectrum and determine the chemical composition of substances.

2.3. Coating performance measurement

A microhardness tester (EM500-2A, China, Hengyi Shanghai) was employed to measure the microhardness distribution along the vertical direction in the cross-section plane (Fig. 1, hardness measure matrix). A 300 gf load was exerted on the cross-section and held for 12 s. The distance interval between two points was set as 100 μ m. Wear tests were carried out by a MFT-4000 wear test machine (Huahui, Lanzhou, China) and the measurement parameters were list here: t (wear time) = 100 min, s (reciprocating distance) = 5 mm, ν (reciprocating speed) = 200 mm/min, F (test load) = 10 N (a 1 Kg weight was used for loading). A ZrO_2 ceramic ball (HRC >90) was used for dry grinding under room

 Table 2

 Component content of composite materials (wt. %).

No.	Component content (wt %)					
	Ni204	Ti	С	NbC		
1#	70	0	0	30		
2#	70	24	6	0		
3#	70	12	3	15		
4#	70	7	2	21		
5#	70	0	5	25		

Table 1 Chemical composition of Ni204 powder and #45 die steel (wt. %).

	С	P,S	Si	Cr	Ni	Mn	Mo	Nb	Cu	Fe
Ni204	≤0.03	_	0.4	21	Bal.	-	9	4	_	1.5
45 steel	0.42-0.5	≤0.045	0.17-0.37	≤0.25	≤0.25	0.5-0.8	-	-	≤0.25	Bal.

Table 3Laser cladding parameters.

No.	Process parameters							
	Laser powers (W)	Scan speed (mm/s)	Powder feeding rate (r/min)	overlap rate (%)	Δz (mm)			
1# 2#	450	5.5	0.7	35	0.35			
3#								
4#								
5#								

temperature (RT, 298 K), the diameter is 5 mm. Before and after wear testing, the polished coating surface was cleaned with alcohol.

3. Results and discussion

3.1. Coating phase analysis

The diffraction peaks of samples are shown in Fig. 2. The results show that all samples are primarily composed of (Fe, Ni), Ni–Cr–Mo–Nb, and Ni–Cr–Fe. Aside from sample 1#, the diffraction peaks of MC (M = Ti, Nb, Mo, Fe, Cr) were detected in other samples [19,34,35]. The diffraction peaks of NbC appeared in samples 1# and 5#, and the new diffraction peaks of TiC, (Ti, Nb) C and (Fe, Cr) were detected in samples 2#–4#. When adding Ti and C particles in the Ni204 coating, TiC and (Ti, Nb) C are in-situ synthesized. It is well known that the nucleation capacity of the phases in the liquid phase depends on the Gibbs free

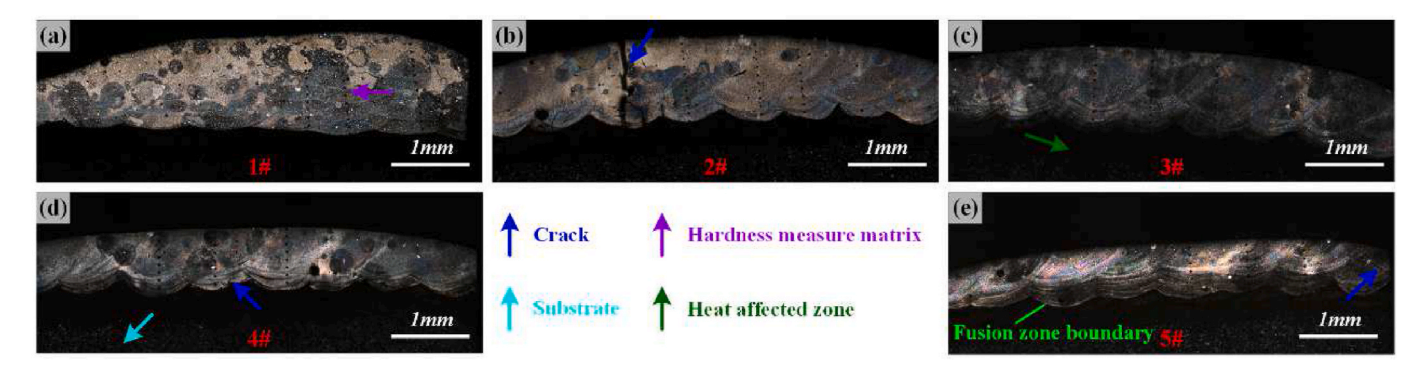


Fig. 1. Cross-section morphology of coatings. (a) Sample 1#; (b) Sample 2#; (c) Sample 3#; (d) Sample 4#; (e) Sample 5#.

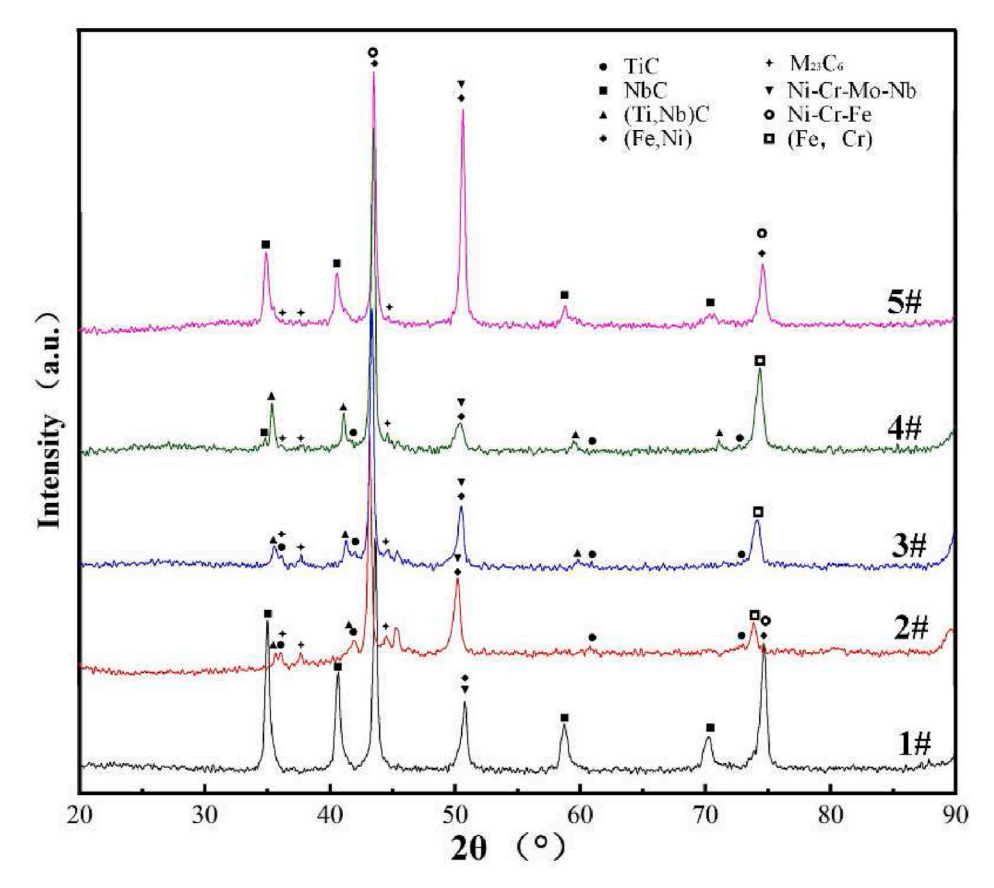


Fig. 2. XRD patterns of coatings with different Ti-C-NbC ratios.

energy generated by these phases. The absolute value of Gibbs free energy of TiC (Gibbs free energy is -158.7 J/mol at 2100 K) is greater than NbC (Gibbs free energy is -137.510 J/mol at 2100 K) [36]. Therefore, TiC nucleated initially, prior to NbC was induced to attach to the TiC phase. The fluctuation of the Ti/Nb ratio makes TiC and NbC alternative generated, the changing Ti/Nb ratio promoted the formation of (Ti, Nb) C [19]. Cr₂₃C₆ and Cr₇C₃ are precipitated before Cr₃C₂, Fe and Ni elements can replace Cr element in the cubic crystal structure of Cr₂₃C₆ [35]. According to Ti-C and C-Cr phase diagrams, TiC precipitation temperature (3000 $^{\circ}\text{C})$ is higher than the Cr–C compound (lower than 1800 °C) [37]. TiC and NbC have a lot of matching surfaces with very low free energy [22]. With the temperature reduced, the previously formed TiC particles become the most potential attachment point to form (Ti, Nb) C phases. Then, MC compounds precipitated. As the temperature continued to fall, (Fe, Ni) solid solution and other phases precipitated.

3.2. Coating composition and microstructure analysis

The distribution of Nb, C, Ti, Mo, Cr, Fe, and Ni elements in sample 3# is given in Fig. 3. Cr, Fe, and Ni are simultaneously detected in the matrix. In the final stage of solidification, a small number of metal atoms in the liquid phase formed the eutectic structures with (Fe, Ni) [2,21]. The matrix primarily contains (Fe, Cr) solid solutions, (Fe, Ni) solid solutions and Fe–Cr–Ni phases (see XRD results in Fig. 2). According to Fig. 3(a)–(e), the strengthening phases in coatings 3# primarily contain Ti, Nb, Mo, and C, indicating in-situ synthesis of (Ti, Nb) C binary ceramic phases. Mo gathered around (Ti, Nb) C particles, forming the (Ti, Nb, Mo) C multiphase [15]. From Fig. 3(b)–(e), these carbide particles are essentially Ti-riched in the middle and Nb riches in the periphery, and Mo elements gather around Nb, forming core-shell structure multiphase.

Fig. 4 illustrates the interface characteristics between the substrates and coatings. The obvious interface in the substrate and coating appeared in the metallurgical bonding zone of the molten pool and substrate. The formation of thin bands indicates good metallurgical bonding [23,38]. During the cladding process, NbC aggregates in the coating, forming the Chinese-script structures, as shown in Fig. 4(a). When NbC and C particles are added to the coating, the Chinese-script structures disappeared, as shown in Fig. 4(e). From Fig. 2, the diffraction peaks of MC (M = Fe, Cr, Mo, Nb) indicate that the C elements react with M in the coating. Multi carbides (Fe, Cr, Mo, Nb) C and in-situ synthesized NbC are formed. Free Nb decreases in the molten pool, Mo is preferred to gather around NbC and hinders coarsening of carbides

[34]. Compared with other research [16], the aggregation phenomenon of TiC is disappeared, and the distribution of in-situ synthesized TiC in the coatings is more uniform.

When adding Ti and C particles, it is clear that the (Ti, Nb) C, TiC and NbC (see Fig. 2) ceramic phases are formed in the coatings 3# and 4# (Fig. 4(c) and (d)). The Chinese-script structures disappear and promote the carbide particle dispersion distribution [22,23]. According to thermodynamics, the TiC is more accessible to form than NbC. As the crystal nucleus of NbC, in-situ synthesized TiC particles promoted the precipitation of Ti and Nb complex carbides [20]. The priority formed TiC particles are dispersed in the coatings. Therefore, the microstructures are refined by adding Ti and C particles.

According to the distribution of Nb, Mo, Cr, Ni, and C in the Chinese-script structures phase and matrix of sample 1# (Fig. 5), Nb, Mo, and C are detected in the Chinese-script structures, which is confirmed as NbC (Combining with Fig. 2). Mo dissolved in NbC to form (Nb, Mo) C [34].

Figs. 6 and 7 are the SEM and BSE images of samples, respectively. The microstructure of coatings with various Ti/C/NbC mass friction ratios are quite different. Aside from sample 1#, no Chinese-script structures are found. The distribution of NbC particles in the coating 5# (Fig. 6(e)) is more uniform than coating 1#, and the size of strengthening phases decreased. By adding C particles, highly interconnected network structures are formed between NbC particles [39]. Fig. 6(b) shows the microstructure of sample 2#. The in-situ synthesized TiC particles (the gray phases in Fig. 6(b)) are dispersively distributed in the coating [15,16].

In the laser cladding process, Ni-based alloys melt first to form Ni-based alloy solutions due to their low melting point. Ti and Nb elements are redistributed under the influence of interfacial tension gradients. During the solidification stage, the in-situ synthesized TiC preferentially precipitates and acts as the core of NbC [19,22]. The in-situ synthesized TiC, (Ti, Nb) C and MC compounds promote the nucleation of the coatings. Therefore, the strengthening phases of samples 3# and 4# (Fig. 6(c) and (d)) are uniformly distributed in the coating. At the same time, the preferentially precipitated strengthening phase obstructs element diffusion, improves temperature gradient, and refines microstructure.

It is noticed that the remarkable core structures appeared in Fig. 7(b) and the milky white phases in Fig. 7(a) and (c) are NbC. When adding C and NbC particles, a large number of compounds appeared between NbC particles. When adding Ti, C, and NbC particles, TiC preferentially precipitates, followed by NbC [19]. In the core structures, the central area of core structure enriches the Ti element, the intermediate area enriches Nb elements and the outermost area enriches with Mo [23,34].

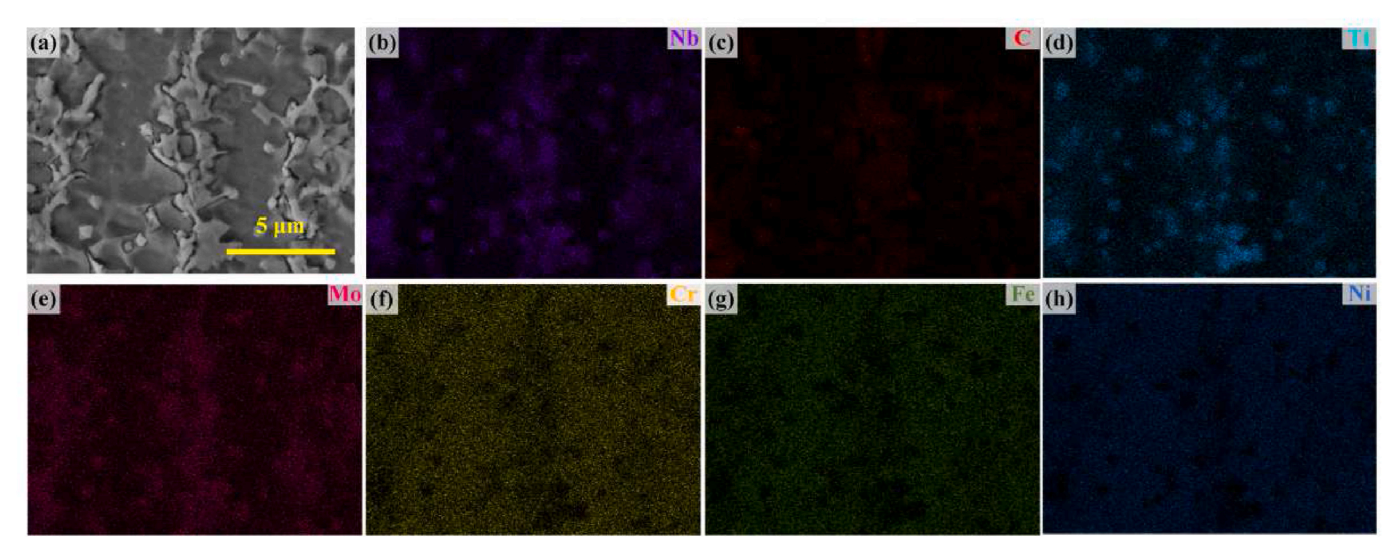


Fig. 3. EDS mappings of the distribution of Nb, C, Ti, Mo, Fe, Cr, and Ni in sample 3#.

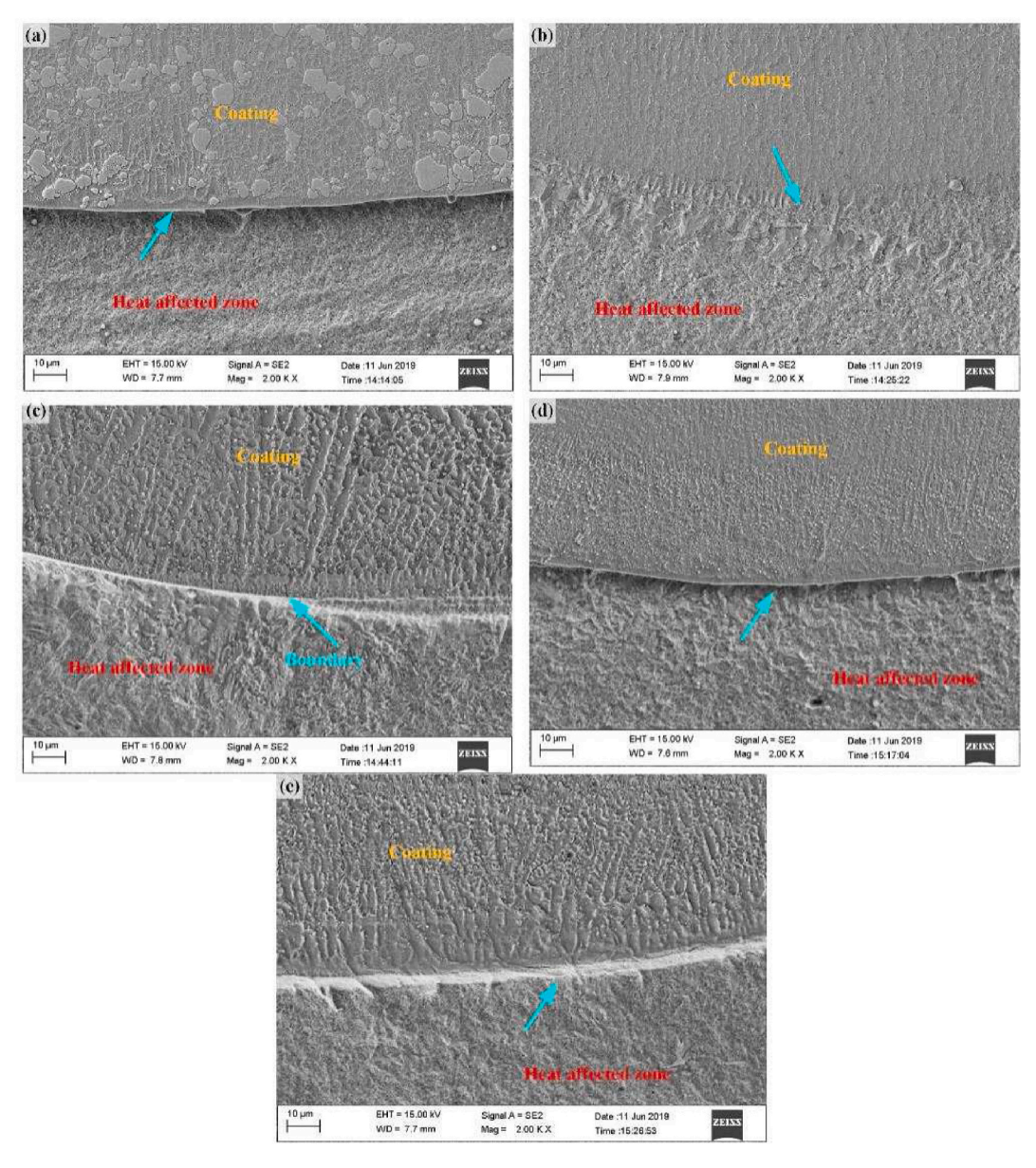


Fig. 4. The microstructure of coatings around the interface of 45 steel substrate and coating (a) Sample 1#; (b) Sample 2#; (c) Sample 3#; (d) Sample 4#; (e) Sample 5#.

The phases at points 1-9 in Fig. 6 are further analyzed by energy spectrum analysis, and the elemental content at points 1-9 are shown in Table 4. In solidification, not all Ti was used to form TiC. Some Ti remained in the matrix, forming NiTi [24]. Energy spectra 2, 6, and 8 regions indicate the main presence of Fe, Ni and Cr, and other elements (Ti, Mo, Nb) dissolved in these matrix regions. Combining with Figs. 2 and 3, the phases in regions 2 and 8 are [Fe, Ni] solid solutions and Fe-Cr-Ni, and [Fe, Cr] solid solutions, [Fe, Ni] solid solutions and Fe-Cr-Ni in region 6 [40,41]. Compared with samples 2#-4#, the more C particles in samples 1# and 5# could react with the Cr element. The diffraction peaks of [Fe, Cr] were not detected in samples 1# and 5#. Point 1 primarily contains Ti, C, Ni, Fe, Cr. From the XRD results in Fig. 2, the gray phases are TiC and MC_x (M = Fe, Ni, and Cr) [15,16,35]. At points 3-5, Ti, C, and Nb are the predominant elements. According to XRD results in Fig. 2, EDS maps results in Fig. 3, confirming the in-situ synthesis of TiC and (Ti, Nb) C ceramic phases. Point 7 is a lump structure strengthening phase of the coating, where the predominant elements are Nb and C, indicating the phase is NbC. Nb, C, Ni, Cr, and Fe are the predominant elements at point 9. The results from sample 5# in Figs. 2 and 7 show that the strengthen phases were MC_x (M = Ni, Fe and Cr).

3.3. Microhardness of the composite coating

The microhardness of the Ni-based coatings reinforced with various content of Ti, C, and NbC particles was measured, the microhardness distribution along the depth direction is shown in Fig. 8. The results show that the Ti, C, and NbC have a remarkable effect on the microhardness of the coatings. Sample 2# exhibites higher microhardness than other coatings, which is about $485.7~{\rm HV_{0.3}}$. In the early work [16], the microhardness of 30% ex-situ TiC adding into Ni204 alloy coating is $2.0~{\rm factors}$ larger than that of sample 2#. In this study, the distribution of strengthening phases is more uniform, so microhardness fluctuation in the coating is relatively small. The size of in-situ synthesis ceramic particles is smaller and more even distributed than ex-situ ceramic particles. The discontinuous in-situ reinforcing larger phase could increase the wear resistance, while continuous and refined ceramic phases seem to be a more desirable structure [19]. NbC particles are softer than

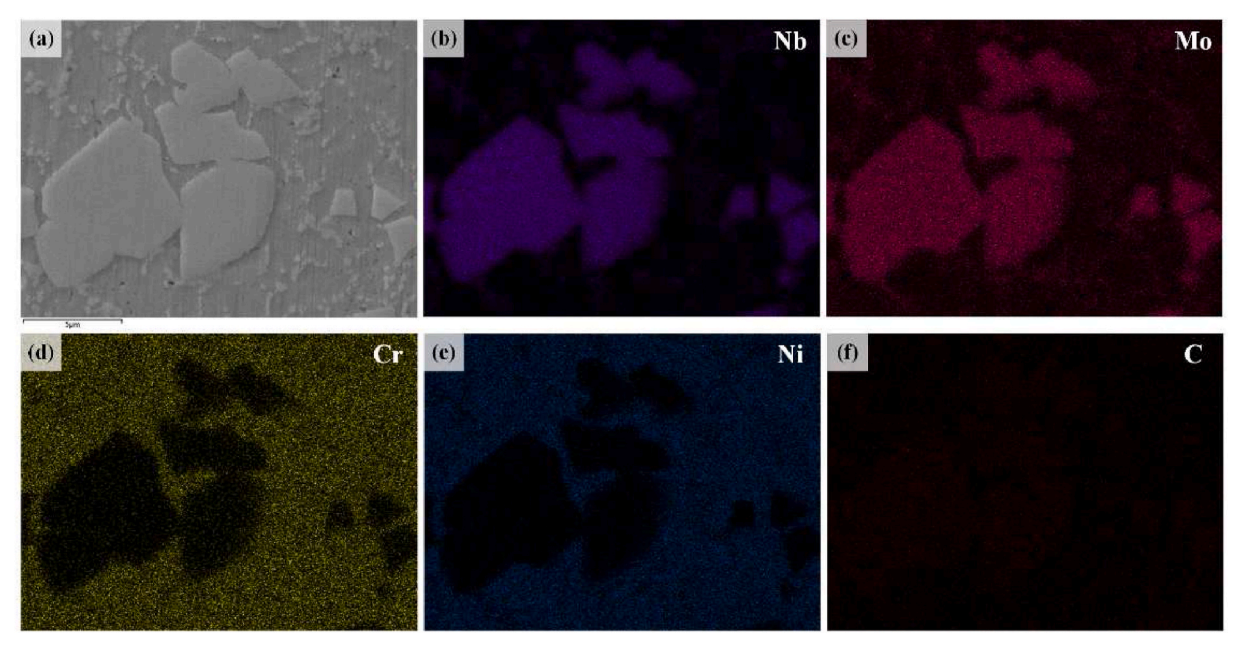


Fig. 5. EDS mapping of distribution of Nb, C, Mo, Cr, and Ni in sample 1#.

TiC, and the NbC phases with lump structure are extremely detrimental to the stability of performance. The in-situ synthesized TiC particles more uniformly distributed in the sample 2# coating, refined the microstructures [9]. Adding the same mass fraction of reinforcing particles, in-situ synthesized TiC phases have the most remarkable reinforcement on the microhardness of Ni-based alloy coatings. When adding ex-situ NbC particles, the microhardness of sample 1# is 456.8 HV_{0.3}, which is higher than samples 3# and 4# (adding Ti particles in the coatings). The reason for this phenomenon may be that the Chinese-script structures have been proven to be able to better distribute compression forces and provide more structural support for the soft matrix than the discrete particles. Sample 3# has more in-situ synthesis (Ti, Nb) C ceramic phases than sample 4#. Therefore, sample 3# coating shows higher microhardness. In addition, the coating has a higher hardness ratio of the hard phase to the soft phase could cause the properties of the soft phase to take a leading role in microhardness distribution, especially at the low content of hard particles [42]. When the adding content of Ti is low, ex-situ NbC content plays an important role in the deformation resisting capability. The appearance of new carbides MC_x (M = Cr, Ni, Fe) also contributed to refining microstructure, increasing microhardness. Therefore, the microhardness of composite coatings with 25% NbC +5% C is higher than the coatings with 7% Ti +2% C +21% NbC. The content and morphology characteristics of the reinforcement phase are responsible for the microhardness of coatings. Aside from coating 2#, the coatings present a small microhardness difference between the top and bottom. The TiC floating problems are resolved by the addition of NbC particles.

3.4. The friction coefficient of the composite coating

In general, the microstructure and strengthening phase characteristics significantly affect both the wear resistance and microhardness of the coatings [43,44]. The relationship of friction coefficients with time was developed through the addition of different content of Ti, C, and NbC particles, as shown in Fig. 9. The (Fe, Ni) and (Fe, Cr) solid solutions in the composite coatings play the role in the binder, providing a degree of toughness, and it also acts as the framework for TiC, NbC, (Ti, Nb) C, and other strengthen phases. The friction coefficients of all samples fluctuated strongly in the initial stage, but the fluctuation is short-lived and only lasted 20 min. The average friction coefficient between 20 and

100 min of the whole test time is used to reflect the friction coefficient of the samples. The dispersive distribution and continuous reinforcement phases could better disperse load during the wear stage, so the friction coefficient of sample 2# is the lowest, followed by samples 3#, 5#, 1# and 4#. It is noticed that sample 2# shows the smallest friction coefficient of 0.597, which is slightly higher than the previous study [16]. The results of the wear experiment show that it is useless to use hardness to reflect wear resistance. Because the wear resistance and microhardness of the coating might relate to the strengthen phase characteristics. According to the results in Figs. 6 and 9, carbides have a positive effect on wear resistance, hiding the coating matrix peeling. Due to the reinforcement of Ti to the coating, the refinement microstructure increased the support ability of the matrix to the strengthening phase. The (Ti, Nb) C can improve the toughness of the matrix, and have better bonding with the matrix than NbC and TiC [22,37]. Therefore, the suitable Ti and C/NbC ratio is beneficial to the improvement of wear resistance.

Fig. 10 shows the two-dimension wear morphologies of the sample. The deep furrow scratches and material adhesion are observed in the Ni204 composite coatings. One can infer that adhesive and abrasive wear occurred in samples 1# and 3#-5# (Fig. 10(a) and (c) to 10(e)), and abrasive wear occurred in sample 2# (Fig. 10(b)). During the wear process, part of the soft bonding phases ((Fe, Ni) and (Fe, Cr) solid solution) and in-situ synthesis of hard phases (TiC, NbC, MCx and (Ti, Nb) C) were peeled. The plastic flow and secondary welding of detritus and grinding debris occurred after repeated grinding and friction of the ZrO₂ ball. This is a typical adhesion mechanism. The exfoliated carbide particles serve as the wear medium between the coating and the ball. As the wear processing continues, the peeled hard particles scratched the surface generated shallow furrow grooves [21]. The adhesion phenomena of samples 2# and 3# are not as serious as the samples 1#, 4# and 5#. The in-situ synthesis TiC and (Ti, Nb) C promote nucleation of coating, refine microstructure and improve the supportability of the matrix to the strengthening phases. In sample 1#, the higher hardness ratio of ex-situ NbC and matrix causes the matrix to peel easily [42]. The serious adhesion phenomena are detrimental to wear resistance. The MC_x (M = Fe, Cr and Ni) carbides ratio formed in sample 5# is the most. Not all Ti atoms in sample 4# are in-situ synthesized TiC with C. Some Ti elements would dissolve in the matrix. Compared with sample 5#, the reinforcing effects of MCx and ex-situ NbC are better than in-situ TiC and (Ti, Nb) C, and ex-situ NbC in sample 4#. The carbides content and matrix

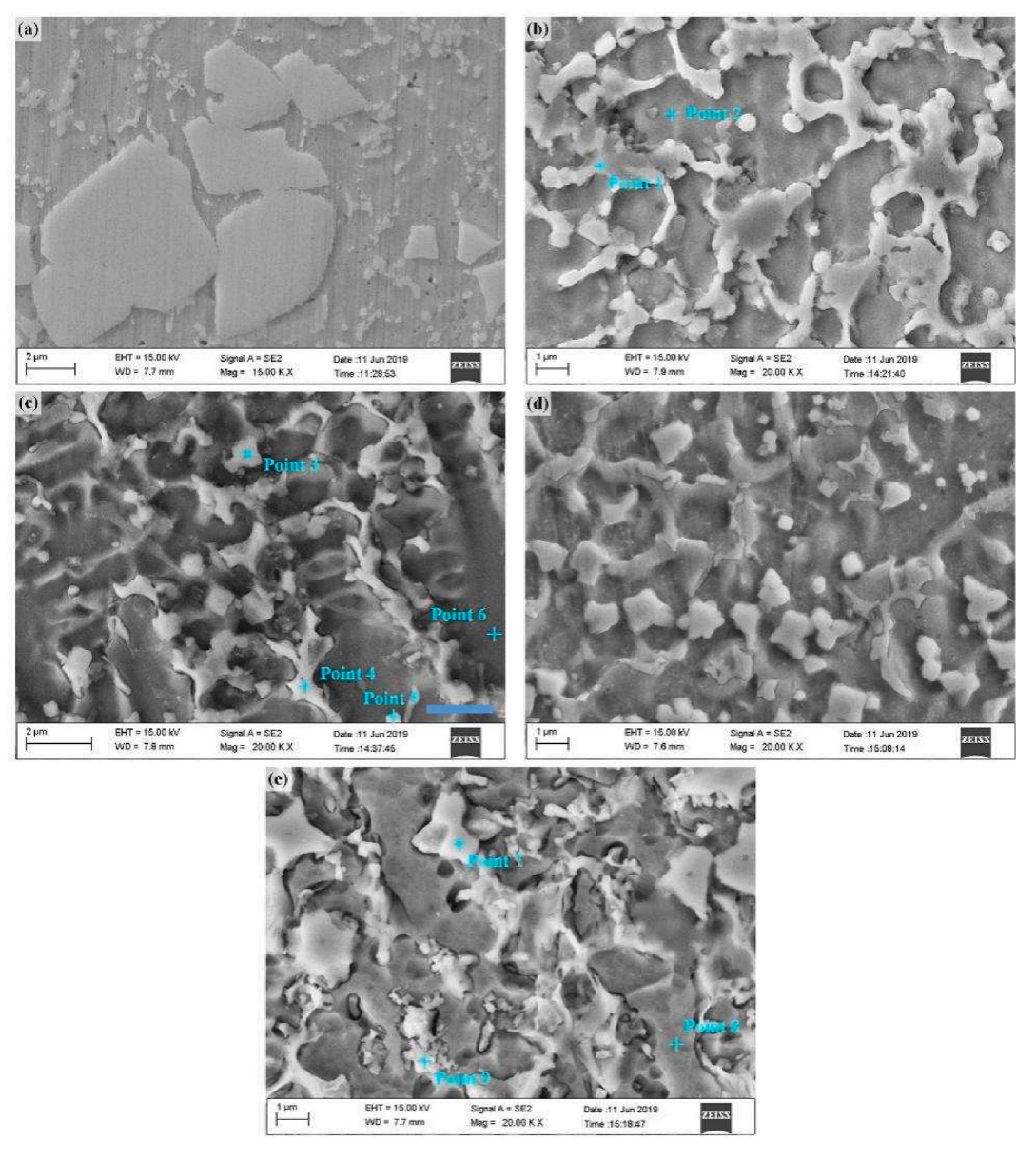


Fig. 6. SEM images of coatings. (a) Sample 1#; (b) Sample 2#; (c) Sample 3#; (d) Sample 4#; (e) Sample 5#.

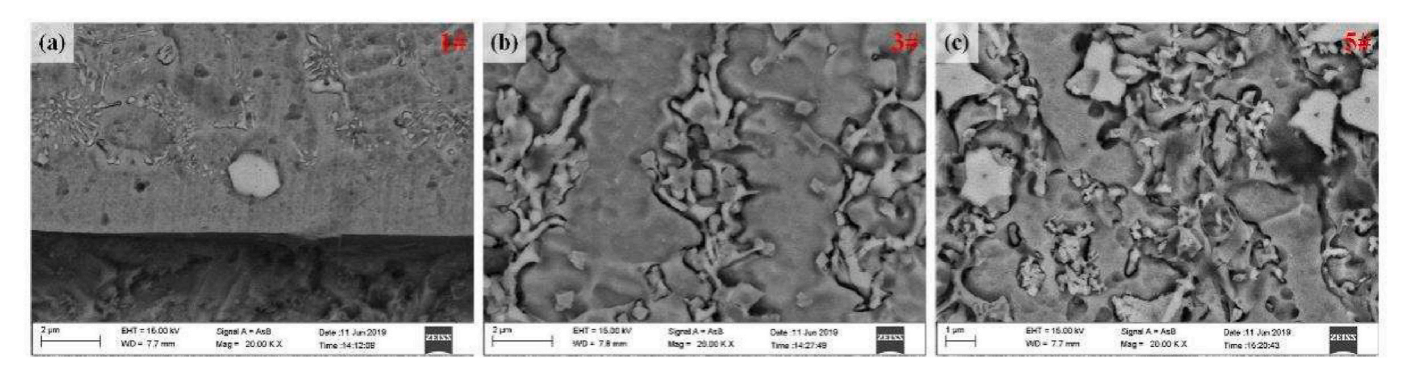


Fig. 7. BSE images of coatings. (a) Sample 1#; (b) Sample 3#; (c) Sample 5#.

composition played a decisive role.

The cross-section morphology of wear scratch and the height and width of wear scratches are shown in Fig. 11 and Table 5, respectively. The cross-section wear area is not positively correlated with the friction

coefficient. The friction coefficient can only represent the use of good lubrication performance does not represent wear resistance. Sample 1# has the smallest cross-section wear area of 2716.42 μm^2 under 100 min wear time. The in-situ ceramic phases are dispersive and evenly

 Table 4

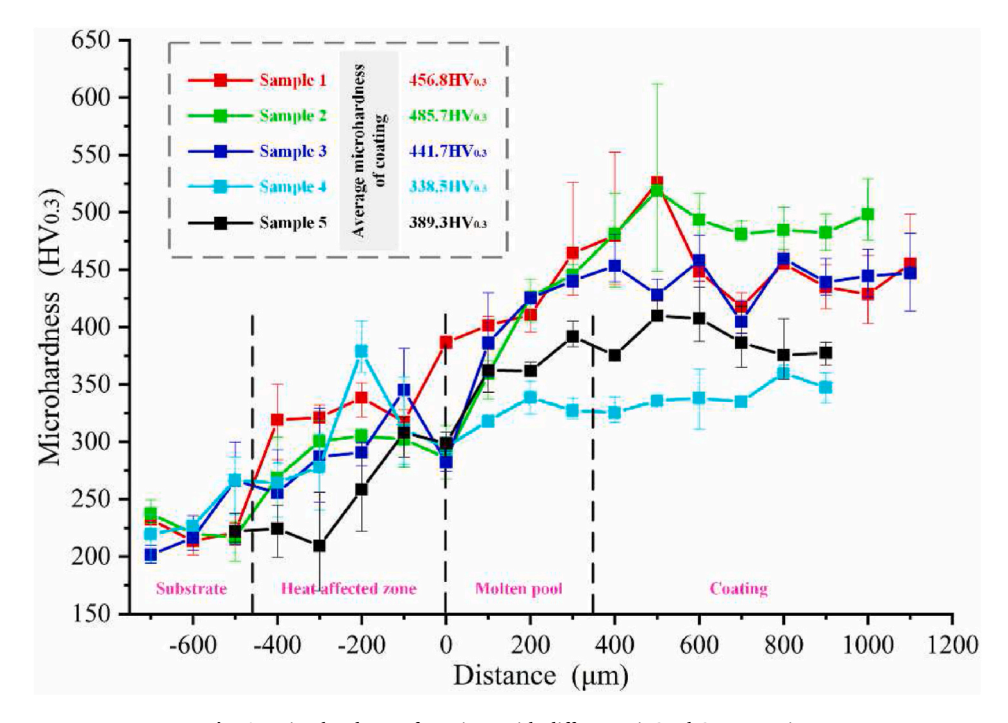
 EDS spectra analyses results of samples (au. %).

Marl	xed locations	Ti	С	Nb	Mo	Ni	Cr	Fe
2#	Point 1	8.78	52.76	1.12	2.43	13.26	5.63	14.70
	Point 2	3.88	48.68	0.24	1.45	17.15	7.76	20.15
3#	Point 3	19.8	53.40	7.15	1.78	3.8	2.67	4.42
	Point 4	16.85	47.23	6.79	2.69	7.37	4.12	7.26
	Point 5	14.55	52.95	4.90	1.92	6.78	3.83	8.12
	Point 6	3.28	14.11	0.51	2.21	31.76	13.95	31.85
5#	Point 7	0.40	67.47	22.02	4.44	1.08	3.59	1.00
	Point 8	_	51.09	0.76	1.34	22.94	7.62	15.80
	Point 9	0.25	59.31	11.61	2.50	9.41	5.32	7.54

distributed in the coating, refine the microstructure, and improve the properties. The large Chinese-script structures NbC required a deeper grinding depth of the matrix to remove these strengthening phases. Therefore, the NbC phases emerged with the matrix wearing off. The bare NbC further hinders matrix spalling, improving the coating wear resistance.

4. Conclusion

In this study, various Ti/C/NbC mass ratio composite coatings were built on the 45 steel via laser cladding. In-situ synthesis TiC, (Ti, Nb) C and MCx strengthen phases and carbides reinforced the mechanical properties. The frontier conclusions are listed here.



 $\textbf{Fig. 8.} \ \ \textbf{Microhardness of coatings with different Ti/C/NbC mass ratio.}$

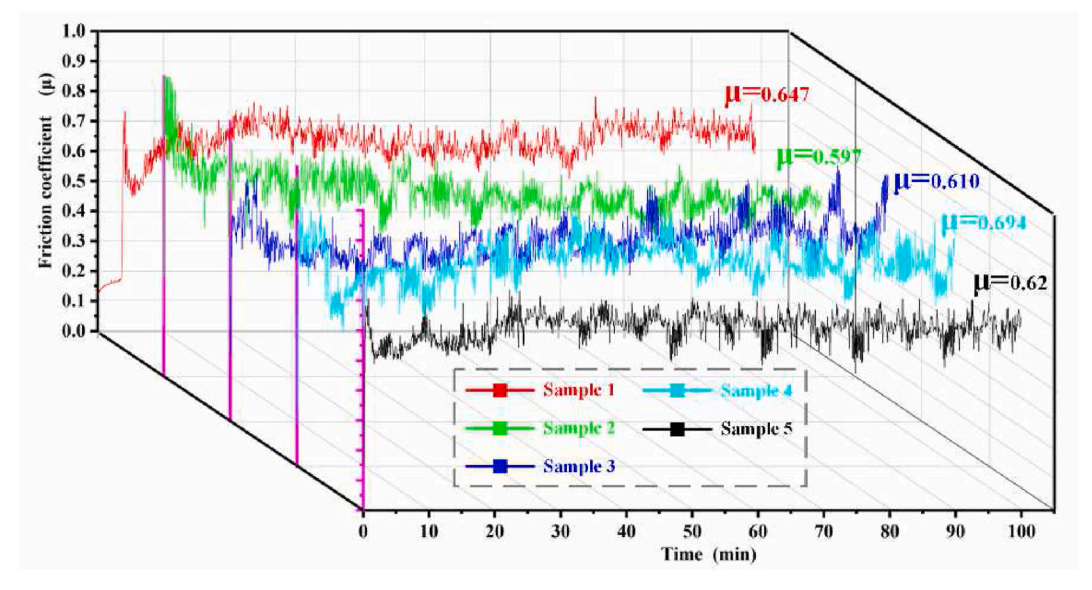


Fig. 9. Friction coefficient-time curves of different samples.

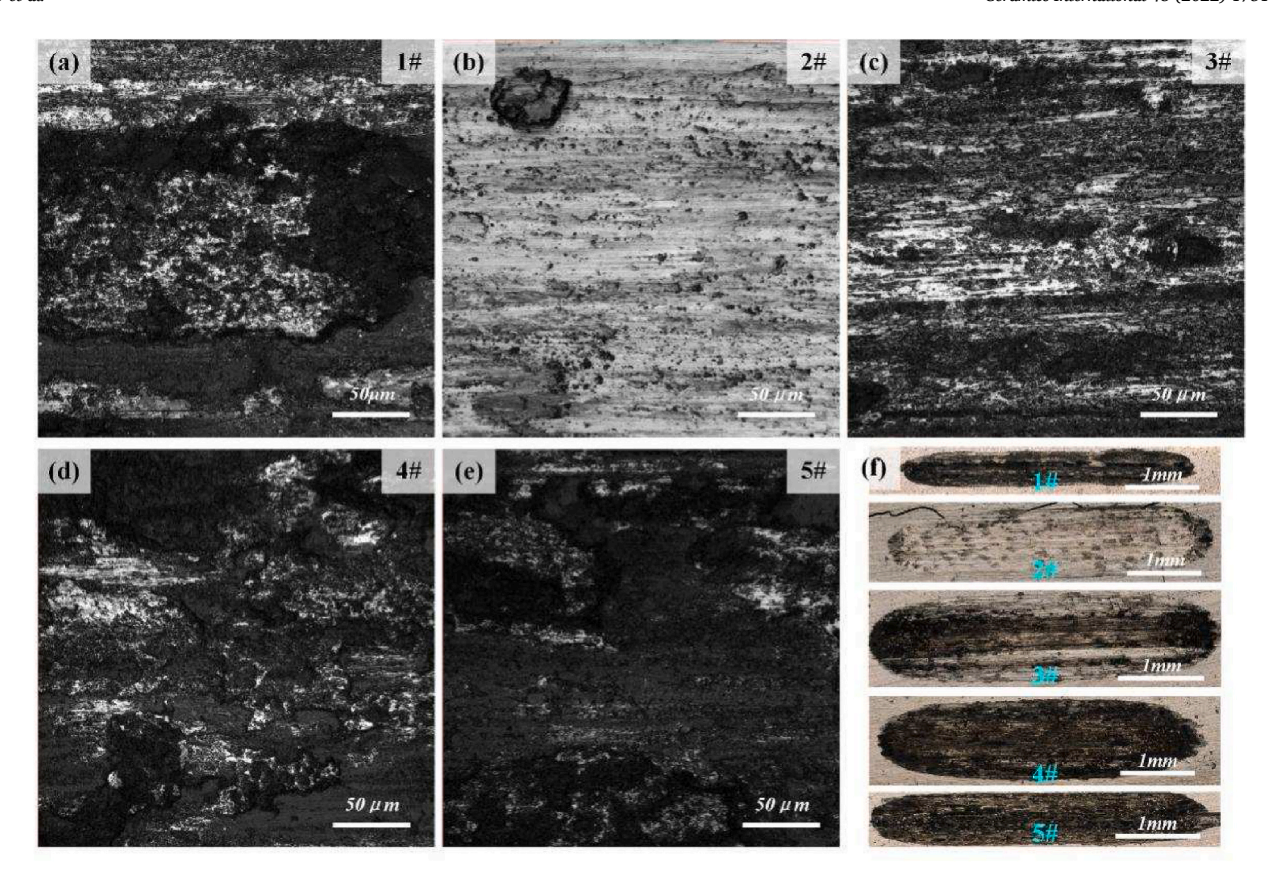


Fig. 10. Wear morphologies of different samples.

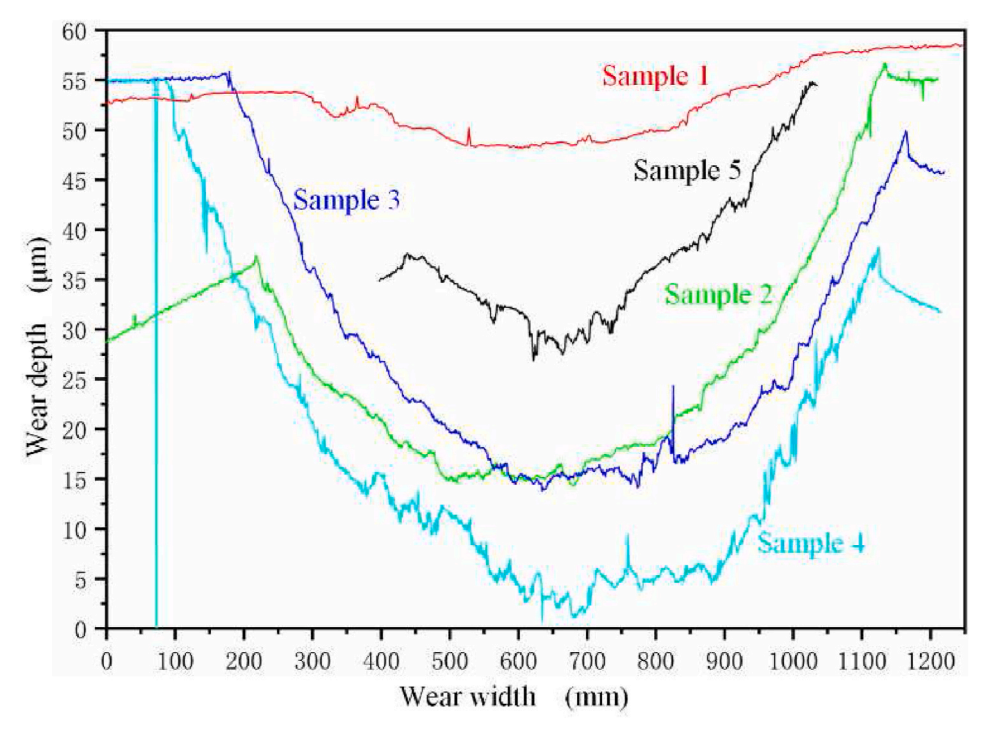


Fig. 11. Cross-section morphology of wear scratch.

- (1) The addition of Ti and C particles contributes to the remarkable Chinese-script structures NbC disappeared. The TiC and NbC were alternately formed and generated in-situ (Ti, Nb) C particles. The in-situ ceramic phases (TiC and (Ti, Nb) C) and carbides
- $(\mbox{MC}_{\mbox{\tiny X}},\,\mbox{M} = \mbox{Fe},\,\mbox{Ni},\,\mbox{Cr})$ contributed to grains refinement and uniform distribution.
- (2) The enhancement of TiC on the microhardness of the coating is more than NbC and in-situ (Ti, Nb) C, and the microhardness of

Table 5 Characteristics of wear morphology (μm).

Sample	Height (μ	ım)		Width (µm)	Area (μm²)
	Right	Left	Average		
1#	4.74	9.51	7.12	647.65	2716.42
2#	41.09	22.70	31.89	912.32	20116.32
3#	40.91	29.51	35.21	957.26	25888.69
4#	51.51	34.74	43.12	1044.96	30556.09
5#	9.02	26.28	17.65	595.12	5704.48

the coating is both related to the content of the reinforcing phase and the hardness ratio of the matrix to the reinforcing phases. The composite ceramic coating with 24% Ti + 6% C exhibited the largest microhardness with 485.7 HV $_{0.3}$. The in-situ (Ti, Nb) C solves the TiC floating up and reduces the hardness difference in the coating.

(3) The high support capacity of the matrix to the hard phase improves the wear resistance. The lump structures of the strengthening phase are positively correlated with wear resistance, and refinement microstructure. Besides, uniform distribution of strengthening phases has a positive effect on the friction coefficient. When 15% NbC +12% Ti + 3 % C is added, the coating shows excellent combination properties: microhardness, wear resistance, and friction coefficient.

Declaration of competing interest

The authors declare that they have no known competing financial interests or personal relationships that could have appeared to influence the work reported in this paper.

Acknowledgment

This work was supported by the Ministry of Industry and Information Technology of China under Grant (No. 201675514).

References

- B. Ye, Y. Chu, K. Huang, D. Liu, Synthesis and characterization of (Zr1/3Nb1/3Ti1/3)C metal carbide solid-solution ceramic, J. Am. Ceram. Soc. 102 (2019) 919–923, https://doi.org/10.1111/jace.16141.
- [2] Q. Li, Y. Lei, H. Fu, Growth mechanism, distribution characteristics and reinforcing behavior of (Ti, Nb)C particle in laser cladded Fe-based composite coating, Appl. Surf. Sci. 316 (2014) 610–616, https://doi.org/10.1016/j.apsusc.2014.08.052.
- [3] P. Farahmand, S. Liu, Z. Zhang, R. Kovacevic, Laser cladding assisted by induction heating of Ni-WC composite enhanced by nano-WC and La2O3, Ceram. Int. 40 (2014) 15421–15438, https://doi.org/10.1016/j.ceramint.2014.06.097.
- [4] X.B. Liu, X.J. Meng, H.Q. Liu, G.L. Shi, S.H. Wu, C.F. Sun, M. Di Wang, L.H. Qi, Development and characterization of laser clad high temperature self-lubricating wear resistant composite coatings on Ti-6Al-4V alloy, Mater. Des. 55 (2014) 404–409, https://doi.org/10.1016/j.matdes.2013.09.038.
- [5] C.P. Paul, S.K. Mishra, P. Tiwari, L.M. Kukreja, Solid-particle erosion behaviour of WC/Ni composite clad layers with different contents of WC particles, Opt Laser. Technol. 50 (2013) 155–162, https://doi.org/10.1016/j.optlastec.2013.03.002.
- [6] Z. Tong, X. Ren, J. Jiao, W. Zhou, Y. Ren, Y. Ye, E.A. Larson, J. Gu, Laser additive manufacturing of FeCrCoMnNi high-entropy alloy: effect of heat treatment on microstructure, residual stress and mechanical property, J. Alloys Compd. 785 (2019) 1144–1159, https://doi.org/10.1016/j.jallcom.2019.01.213.
- [7] Y. Sun, L. Jin, Y. Gong, X. Wen, G. Yin, Q. Wen, B. Tang, Experimental evaluation of surface generation and force time-varying characteristics of curvilinear grooved micro end mills fabricated by EDM micro texture, J. Manuf. Process. 73 (2022) 799–814, https://doi.org/10.1016/j.jmapro.2021.11.049.
- [8] R.M. Genga, G. Akdogan, J.E. Westraadt, L.A. Cornish, Microstructure and material properties of PECS manufactured WC-NbC-CO and WC-TiC-Ni cemented carbides, Int. J. Refract. Metals Hard Mater. 49 (2015) 240–248, https://doi.org/10.1016/j. iirmhm.2014.07.030.
- [9] K. Yang, Y. Gao, K. Yang, Y. Bao, Y. Jiang, Microstructure and wear resistance of Fe-Cr13-C-Nb hardfacing alloy with Ti addition, Wear 376–377 (2017) 1091–1096, https://doi.org/10.1016/j.wear.2016.12.062.
- [10] L. Yang, T. Yu, M. Li, Y. Zhao, J. Sun, Microstructure and wear resistance of in-situ synthesized Ti(C, N) ceramic reinforced Fe-based coating by laser cladding, Ceram. Int. 44 (2018) 22538–22548, https://doi.org/10.1016/j.ceramint.2018.09.025.

- [11] W. Zhang, Y. Du, Y. Peng, Effect of TaC and NbC addition on the microstructure and hardness in graded cemented carbides: simulations and experiments, Ceram. Int. 42 (2016) 428–435, https://doi.org/10.1016/j.ceramint.2015.08.127.
- [12] J. Hashim, L. Looney, M.S.J. Hashmi, Metal matrix composites: production by the stir casting method, J. Mater. Process. Technol. 92–93 (1999) 1–7, https://doi.org/ 10.1016/S0924-0136(99)00118-1.
- [13] S.A. Sajjadi, H.R. Ezatpour, H. Beygi, Microstructure and mechanical properties of Al-Al2O3 micro and nano composites fabricated by stir casting, Mater. Sci. Eng. 528 (2011) 8765–8771, https://doi.org/10.1016/j.msea.2011.08.052.
- [14] A.K. Srivastava, K. Das, Microstructure and abrasive wear study of (Ti,W)C-reinforced high-manganese austenitic steel matrix composite, Mater. Lett. 62 (2008) 3947–3950, https://doi.org/10.1016/j.matlet.2008.05.049.
- [15] Y. Zhao, T. Yu, C. Guan, J. Sun, X. Tan, Microstructure and friction coefficient of ceramic (TiC, TiN and B4C) reinforced Ni-based coating by laser cladding, Ceram. Int. 45 (2019) 20824–20836, https://doi.org/10.1016/j.ceramint.2019.07.070.
- [16] Y. Zhao, T. Yu, J. Sun, S. Jiang, Microstructure and properties of laser cladded B4C/TiC/Ni-based composite coating, Int. J. Refract. Metals Hard Mater. 86 (2020) 105112, https://doi.org/10.1016/j.ijrmhm.2019.105112.
- [17] J. Hashim, L. Looney, M.S.J. Hashmi, Particle distribution in cast metal matrix composites - Part II, J. Mater. Process. Technol. 123 (2002) 258–263, https://doi. org/10.1016/S0924-0136(02)00099-7.
- [18] A.K. Srivastava, K. Das, Microstructural and mechanical characterization of in situ TiC and (Ti,W)C-reinforced high manganese austenitic steel matrix composites, Mater. Sci. Eng. 516 (2009) 1–6, https://doi.org/10.1016/j.msea.2009.04.041.
- [19] W.H. Kan, Z.J. Ye, Y. Zhu, V.K. Bhatia, K. Dolman, T. Lucey, X. Tang, G. Proust, J. Cairney, Fabrication and characterization of microstructure of stainless steel matrix composites containing up to 25 vol% NbC, Mater. Char. 119 (2016) 65–74, https://doi.org/10.1016/j.matchar.2016.07.019.
- [20] K. Yang, K. Yang, Y.F. Bao, Y.F. Jiang, Formation mechanism of titanium and niobium carbides in hardfacing alloy, Rare Met 36 (2017) 640–644, https://doi. org/10.1007/s12598-016-0777-5.
- [21] M. Zhang, M. Li, J. Chi, S. Wang, L. Ren, M. Fang, Microstructure and tribology properties of in-situ MC(M:Ti,Nb) coatings prepared via PTA technology, Vacuum 160 (2019) 264–271, https://doi.org/10.1016/j.vacuum.2018.11.035.
- [22] W.H. Kan, V. Bhatia, K. Dolman, T. Lucey, X. Tang, L. Chang, G. Proust, J. Cairney, A study on novel AISI 304 stainless steel matrix composites reinforced with (Nb0.75,Ti0.25)C, Wear 398–399 (2018) 220–226, https://doi.org/10.1016/j. wear.2017.12.011.
- [23] S. Sun, H. Fu, X. Ping, X. Guo, J. Lin, Y. Lei, W. Wu, J. Zhou, Formation mechanism and mechanical properties of titanium-doped NbC reinforced Ni-based composite coatings, Appl. Surf. Sci. 476 (2019) 914–927, https://doi.org/10.1016/j. apsusc.2019.01.171.
- [24] B. Piekarski, Effect of Nb and Ti additions on microstructure, and identification of precipitates in stabilized Ni-Cr cast austenitic steels, Mater. Char. 47 (2001) 181–186, https://doi.org/10.1016/S1044-5803(01)00166-8.
- [25] A. Emamian, S.F. Corbin, A. Khajepour, Effect of laser cladding process parameters on clad quality and in-situ formed microstructure of Fe-TiC composite coatings, Surf. Coating. Technol. 205 (2010) 2007–2015, https://doi.org/10.1016/j. surfcoat.2010.08.087.
- [26] S. Sun, H. Fu, X. Ping, J. Lin, Y. Lei, W. Wu, J. Zhou, Reinforcing behavior and microstructure evolution of NbC in laser cladded Ni45 coating, Appl. Surf. Sci. 455 (2018) 160–170, https://doi.org/10.1016/j.apsusc.2018.05.199.
- [27] D. Verdi, M.A. Garrido, C.J. Múnez, P. Poza, Cr3C2 incorporation into an Inconel 625 laser cladded coating: effects on matrix microstructure, mechanical properties and local scratch resistance, Mater. Des. 67 (2015) 20–27, https://doi.org/ 10.1016/j.matdes.2014.10.086.
- [28] W.J. Lu, D. Zhang, X.N. Zhang, R.J. Wu, T. Sakata, H. Mori, Microstructure and tensile properties of in situ (TiB + TiC/Ti6242 (TiB:TiC = 1:1) composites prepared of common casting technique, Mater. Sci. Eng. 311 (2001) 142–150, https://doi.org/10.1016/S0921-5093(01)00910-8.
- [29] J.D. Majumdar, B.R. Chandra, A.K. Nath, I. Manna, In situ dispersion of titanium boride on aluminium by laser composite surfacing for improved wear resistance, Surf. Coating. Technol. 201 (2006) 1236–1242, https://doi.org/10.1016/j. surfcoat.2006.01.048.
- [30] Y. bin Cao, S. xin Zhi, Q. Gao, X. tao Tian, T. Geng, X. Guan, C. Qin, Formation behavior of in-situ NbC in Fe-based laser cladding coatings, Mater. Char. 119 (2016) 159–165, https://doi.org/10.1016/j.matchar.2016.08.005.
- [31] B. AlMangour, D. Grzesiak, J.M. Yang, In-situ formation of novel TiC-particle-reinforced 316L stainless steel bulk-form composites by selective laser melting, J. Alloys Compd. 706 (2017) 409–418, https://doi.org/10.1016/j.iallcom.2017.01.149.
- [32] D.N. Hanlon, W.M. Rainforth, C.M. Sellars, Effect of spray forming on the microstructure and properties of a high chromium white cast iron, J. Mater. Sci. 34 (1999) 2291–2301, https://doi.org/10.1023/A:1004573524282.
- [33] G.L.F. Powell, R.A. Carlson, V. Randle, The morphology and microtexture of M7C3 carbides in Fe-Cr-C and Fe-Cr-C-Si alloys of near eutectic composition, J. Mater. Sci. 29 (1994) 4889–4896, https://doi.org/10.1007/BF00356539.
- [34] J.H. Jang, Y.U. Heo, C.H. Lee, H.K.D.H. Bhadeshia, D.W. Suh, Interphase precipitation in Ti-Nb and Ti-Nb-Mo bearing steel, Mater. Sci. Technol. 29 (2013) 309–313, https://doi.org/10.1179/1743284712Y.0000000131.
- [35] H. Okamoto, T.B. Massalski, Binary alloy phase diagrams requiring further studies, J. Phase Equil. 15 (1994) 500–521, https://doi.org/10.1007/BF02649400.
- [36] L. Chen, Y. Zhao, X. Chen, T. Yu, P. Xu, Repair of spline shaft by laser-cladding coarse TiC reinforced Ni-based coating: process, microstructure and properties, Ceram. Int. 47 (2021) 30113–30128, https://doi.org/10.1016/j. ceramint.2021.07.189.

- [37] H.Y. Liu, Z.L. Song, Q. Cao, S.P. Chen, Q. Sen Meng, Microstructure and properties of Fe-Cr-C hardfacing alloys reinforced with TiC-NbC, J. Iron Steel Res. Int. 23 (2016) 276–280, https://doi.org/10.1016/S1006-706X(16)30045-0.
- [38] M. Wang, H. Cui, N. Wei, L. Ding, X. Zhang, Y. Zhao, C. Wang, Q. Song, A new design of in situ Ti(C,N) reinforced composite coatings and their microstructures, interfaces, and wear resistances, ACS Appl. Mater. Interfaces 10 (2018) 4250–4265, https://doi.org/10.1021/acsami.7b17286.
- [39] S.G. Huang, K. Vanmeensel, H. Mohrbacher, M. Woydt, J. Vleugels, Microstructure and mechanical properties of NbC-matrix hardmetals with secondary carbide addition and different metal binders, Int. J. Refract. Metals Hard Mater. 48 (2015) 418–426, https://doi.org/10.1016/j.ijrmhm.2014.10.014.
- [40] E. Pagounis, V.K. Lindroos, Processing and properties of particulate reinforced steel matrix composites, Mater. Sci. Eng. 246 (1998) 221–234, https://doi.org/10.1016/ s0921-5093(97)00710-7.
- [41] D.H. Bacon, L. Edwards, J.E. Moffatt, M.E. Fitzpatrick, Fatigue and fracture of a 316 stainless steel metal matrix composite reinforced with 25% titanium diboride, Int. J. Fatig. 48 (2013) 39–47, https://doi.org/10.1016/j.ijfatigue.2012.09.016.
- [42] H.S. Kim, On the rule of mixtures for the hardness of particle reinforced composites, Mater. Sci. Eng. 289 (2000) 30–33, https://doi.org/10.1016/S0921-5093(00)00909-6.
- [43] D. Yung, A. Zikin, I. Hussainova, H. Danninger, E. Badisch, A. Gavrilovic, Tribological performances of ZrC-Ni and TiC-Ni cermet reinforced PTA hard facings at elevated temperatures, Surf. Coating. Technol. 309 (2017) 497–505, https://doi.org/10.1016/j.surfcoat.2016.11.099.
- [44] Y. Yuan, Z. Li, Microstructure and tribology behaviors of in-situ WC/Fe carbide coating fabricated by plasma transferred arc metallurgic reaction, Appl. Surf. Sci. 423 (2017) 13–24, https://doi.org/10.1016/j.apsusc.2017.06.080.